Global and Planetary Change 148 (2017) 29–41

Contents lists available at ScienceDirect

Global and Planetary Change

journal homepage: www.elsevier.com/locate/gloplacha

Lead–lag relationships between global mean temperature and the atmospheric CO_2 content in dependence of the type and time scale of the forcing

Kirill E. Muryshev[a, b], Alexey V. Eliseev[a, b, c, *], Igor I. Mokhov[a, d], Alexandr V. Timazhev[a, b]

[a] A.M. Obukhov Institute of Atmospheric Physics RAS, Moscow, Russia
[b] Institute of Applied Physics, Russian Academy of Sciences, Nizhny Novgorod, Russia
[c] Kazan Federal University, Kazan, Russia
[d] M.V. Lomonosov Moscow State University, Moscow, Russia

ARTICLE INFO

Article history:
Received 12 April 2016
Received in revised form 9 September 2016
Accepted 8 November 2016
Available online 12 November 2016

Keywords:
Climate change origins
Climate–carbon cycle interactions
Mutual lags
IAP RAS CM

ABSTRACT

By employing an Earth system model of intermediate complexity (EMIC) developed at the A.M. Obukhov Institute of Atmospheric Physics, Russian Academy of Sciences (IAP RAS CM), mutual lags between global mean surface air temperature, T and the atmospheric CO_2 content, q, in dependence of the type and time scale of the external forcing are explored. In the simulation, which follows the protocol of the Coupled Models Intercomparison Project, phase 5, T leads q for volcanically-induced climate variations. In contrast, T lags behind q for changes caused by anthropogenic CO_2 emissions into the atmosphere. In additional idealized numerical experiments, driven by periodic external emissions of carbon dioxide into the atmosphere, T always lags behind q as expected. In contrast, if the model is driven by the periodic non-greenhouse radiative forcing, T leads q for the external forcing time scale $\leq 4 \times 10^2$ yr, while q leads T at longer scales. The latter is an example that lagged correlations do not necessarily represent causal relationships in a system. This apparently counter-intuitive result, however, is a direct consequence of i) temperature sensitivity of the soil carbon stock (which decreases if climate is warmed and increases if climate is cooled), ii) conservation of total mass of carbon in the system in the absence of external carbon emissions, iii) increased importance of the oceanic branch of the carbon cycle at longer time scales. The results obtained with an EMIC are further interpreted with a conceptual Earth system model consisting of an energy balance climate model and a globally averaged carbon cycle model. The obtained results have implications to the empirical studies attempting to understand the origins of the contemporary climate change by applying lead–lag relationships to empirical data.

1. Introduction

According to the available evidence, the Earth system has warmed during the last century: the overall change associated with a trend of the global mean surface air temperature is 0.85 K (with an uncertainty range from 0.65 to 1.06 K) during 1880–2012 and as large as 0.72 K (with an uncertainty range from 0.49 to 0.89 K) during 1951–2012 (Hartmann et al., 2013). The major contribution to this warming is a man-made greenhouse effect with the additional, sometimes compensating contribution of other anthropogenic activities such as release of aerosols and other chemical constituents into the atmosphere, and land use (Bindoff et al., 2013). This is supported by different lines of evidence including empirical models (Lean and Rind, 2008; Mokhov and Smirnov, 2009; Smirnov and Mokhov, 2009; Schönwiese et al., 2010; Mokhov et al., 2012; Canty et al., 2013; Mikšovský et al., 2016) and applications of the fingerprinting technics to simulations with global climate models (Hegerl et al., 1997; Stott et al., 2001; Stone et al., 2007; Stone et al., 2009; Sedlacek and Knutti, 2012; Jones et al., 2013; Ribes and Terray, 2013).

However, other hypothesis for origins of the ongoing climate change exist, in which the major contribution to this change is attributed to natural causes. The most well-known are the hypotheses either explaining this warming as a solar-induced signal

* Corresponding author at: A.M. Obukhov Institute of Atmospheric Physics, Russian Academy of Sciences, 3 Pyzhevsky, Moscow 119017,Russia.
E-mail addresses: kmuryshev@mail.ru (K. Muryshev), eliseev@ifaran.ru (A. Eliseev), mokhov@ifaran.ru (I. Mokhov).

http://dx.doi.org/10.1016/j.gloplacha.2016.11.005
0921-8181/

(e.g., Soon et al., 1996; Idso, 1998; Quinn, 2010; Scafetta, 2012 and references therein) or ascribing it to the unforced natural variability (e.g., Lindzen, 1990). One of the popular arguments in support of these hypotheses is a mutual lag between the temperature and the atmospheric CO_2 content derived from the East Antarctic ice cores: according to these data the CO_2 content lags (rather than leads) temperature (Monnin et al., 2001; Caillon et al., 2003; Mokhov et al. 2005a; Bereiter et al., 2012) by several centuries. Because one typically expects that the effect should lag its cause, this lag was claimed as an evidence against the role of the anthropogenic greenhouse effect in climate change (e.g., Quinn, 2010). This is done despite the results reported for Antarctic ice cores are strictly applicable only for regional temperature rather than to the globally averaged one. In particular, the Antarctic temperature leads the global mean temperature by few millennia during glacial terminations (Stocker and Johnsen, 2003; Schmittner et al., 2003; Ganopolski and Roche, 2009; Shakun et al., 2012).

In addition, Humlum et al. (2013), based on the standard atmospheric measurements data, found that year-to-year increments of the atmospheric CO_2 content lags behind the global mean surface air temperature during 1980–2012. They also claim this as an evidence against the dominant role of anthropogenically induced greenhouse effect in the ongoing climate changes. The paper by Humlum et al. (2013) was critisized at different grounds (Kern and Leuenberger, 2013; Masters and Benestad, 2013; Richardson, 2013), but in the climate skeptics community it is still considered to be important.

Nevertheless, these lags might reflect the internal time scales of the Earth system dynamics rather than implied causality. In particular, it was shown by Masters and Benestad (2013) that q lagging behind T in the Humlum et al.'s (2013) paper is caused by i) their statistical approach neglecting the long-term component of the Earth system response to external forcings, ii) impact of the unforced natural variability on the mutual climate–carbon cycle dynamics. This was demonstrated by using an energy-balance climate model and by a comprehensive Earth system model. However, in both models q was prescribed as a function of time t rather than calculated interactively. As a result, it is sensible to make some steps beyond Masters and Benestad (2013) and to systematically explore this issue by using an Earth system model forced by anthropogenic CO_2 emissions into the atmosphere rather than the prescribed $q(t)$.

More specifically, one may consider a conceptual form of interactions between climate and the carbon cycle (Fig. 1a). For simplicity, all forcings are gathered in two groups: 1) those are related to external, non-CO_2 radiative forcing, and 2) external emissions of carbon dioxide. The former forcings directly affect only physical part of climate and only indirectly impact carbon cycle. In turn, the latter forcings act on carbon cycle, and their impact on the rest of the Earth system is indirect. This conceptual set-up ignores the secondary carbon-containing greenhouse gases (e.g., methane) and the forcings which directly force both climate and the carbon cycle, e.g., land use which changes surface albedo and releases CO_2 into the atmosphere. However, all neglected forcings are not dominant at the global scale during last decades (Myhre et al., 2013).

If the external CO_2 emissions are absent, and the system is driven only by the forcings belonging to the first group (Fig. 1b), one would expect that climate responds to the forcings first and then its response is followed by the carbon cycle response. As a result, one expects that the carbon cycle should lag behind climate change by τ_{CC}.

On the contrary, if the external CO_2 emissions into the atmosphere dominate in the forcing exerted onto the Earth system, the causal chain is principally different from that figured in the previous paragraph. In this case, one expects the carbon cycle response to these emissions is followed by the response of climate. It is expected that climate lags behind the carbon cycle by the value of the order of the time scale τ_C associated with climate response to external forcing (Fig. 1c).

This approach was set to a more specific form by Muryshev et al. (2015), where it was shown that even the simplest globally averaged Earth system model of a commonly used structure is able to replicate these two types of the mutual climate–carbon cycle lag. The principal ingredients needed for this replications are subdivision of the Earth system by two compartments ('climate' and 'the carbon cycle' represented, respectively, by the global mean surface air temperature T and the atmospheric CO_2 content q), each with its own time scale. As a result, different sign of mutual lag between T and q may be obtained depending on the type of the forcing as in Fig. 1b, c.

In the present paper the results obtained in Muryshev et al. (2015) are extended by employing a more elaborate Earth system model belonging to the class of the Earth system models of intermediate complexity, EMICs (Claussen et al., 2002; Petoukhov et al., 2005; Eby et al., 2013; Zickfeld et al., 2013). The simulations with an EMIC are interpreted by using the same conceptual energy balance model as in Muryshev et al. (2015). The latter interpretation is also extended with respect to Muryshev et al. (2015), because in the latter paper all results are reported in a very concise form. We stress that our results are obtained mostly for time scales up to few millennia. Therefore, they are applicable to the ongoing climate change but have no relevance to the Pleistocene glacial cycles which, however, served as a part of motivation for our study.

2. EMIC simulations

2.1. Simulation forced by CMIP5 forcing

In this sections, we report the simulations with the Earth system model of intermediate complexity developed at the A.M. Obukhov Institute of Atmospheric Physics, Russian Academy of Sciences (IAP RAS CM). Its description and performance IAP RAS CM are discussed in Petoukhov et al. (1998), Mokhov et al. (2002), Mokhov et al. (2005b), Eliseev (2011), Eliseev and Mokhov (2011), Eliseev (2012), Mokhov and Eliseev (2012), Eliseev and Sergeev (2014), Eliseev et al. (2014a), Eliseev et al. (2014b), Eliseev et al. (2014c), and Eliseev (2015). In brief, the model contains modules for the atmosphere, the ocean, the Earth land surface, and the terrestrial carbon cycle. The atmospheric module solves equation of heat, moisture, and momentum transport averaged over the typical synoptic temporal (of the order of few days) and spatial (of the order of the Rossby radius of deformation) atmospheric scales with further parametrisation of synoptic scale dynamics (Petoukhov et al., 1998). This module also includes parametrisations of radiative transport in the atmosphere, formation of cloud and precipitation and exchange of heat and moisture between the atmosphere and the Earth surface. An important IAP RAS CM's feature is an assumption of universal (but with distinct vertical scales) exponential profiles for air density and atmospheric specific humidity, and universal linear profile of temperature with a tropospheric lapse rate depending on surface air temperature. In these respects, the IAP RAS CM atmospheric module is similar to that used in the Climber-2 EMIC (Ganopolski et al., 2001; Petoukhov et al., 2000) but has a higher spatial resolution: 4.5° in latitude and 6° in longitude. The IAP RAS CM's equilibrium sensitivity to the doubling of the atmospheric CO_2 content is $\Delta T_{xx} = 2.2$ K.

The IAP RAS CM oceanic module solves equation of heat, moisture, and momentum transport averaged over the typical oceanic synoptic temporal and spatial scales again with parametrised synoptic-scale dynamics. These equation are integrated with respect to depth over the characteristic oceanic layers (well-mixed layer, seasonal thermocline, main thermocline, and the deep ocean) assuming universal profiles of temperature in these layers (for more details, see Petoukhov et al., 1998). We note that the latter

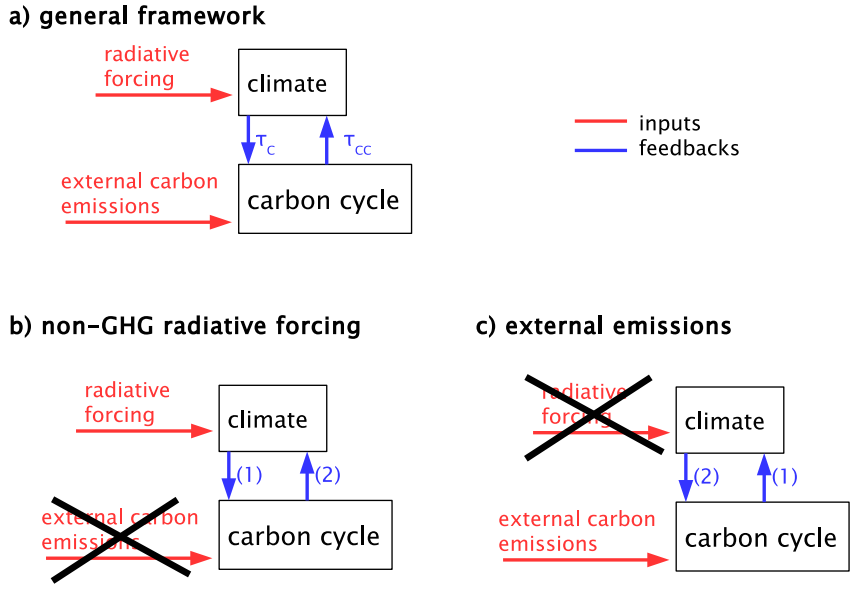

Fig. 1. A general framework of interactions between climate and the carbon cycle (a) and its specific cases for the radiatively, non-greenhouse gases forced system (b), and for the system forced by the external CO_2 emissions (c). All notations are explained in the main text.

assumption might lead to underestimation of oceanic response time scales to external forcing. Oceanic salinity is prescribed.

The basic equations of the Earth surface module are heat diffusion equation and the Richards equation for water infiltration in soil given the heat and moisture fluxes at the soil–atmosphere interface (Eliseev et al., 2009). Among other variables, thus calculated soil water storage are used to drive the carbon cycle module of the IAP RAS CM.

The model's carbon cycle routine was initially reported in Eliseev (2011), Eliseev and Mokhov (2011). The terrestrial part of the model solves annually averaged mass conservation equations for live vegetation and soil carbon stock. This scheme is driven by seasonally resolved meteorological variables and annual mean atmospheric CO_2 content q. Vegetation distribution is prescribed accounting for its subgrid-scale spatial variability (Eliseev and Sergeev, 2014). The latest version of the IAP RAS CM terrestrial carbon cycle is reported in Eliseev (2015). Oceanic carbon cycle module is a Bacastow-type model modified to account for temperature dependence of constants of the oceanic carbonate chemistry (Millero, 1995). In this model, oceanic carbon uptake reads

$$F_o = F_* \cdot \chi \cdot \left[(q - q_0) - \zeta \frac{q_0}{D_0} D \right]. \quad (1)$$

Here D is anomaly of the dissolved inorganic carbon (DIC) in the ocean from its initial value, χ is the CO_2 solubility in the sea water divided by its preindustrial value, $D_0 = 1.5 \times 10^4$ PgC, coefficient F_* is 2.5×10^{-2} PgC yr^{-1} ppmv^{-1}. The dependencies of $\chi(T)$ and $\zeta(q, T)$ are reported in (Mokhov et al., 2008):

$$\zeta(q, T_o) = \zeta_\star \cdot \left(\zeta_1 q_n^2 + \zeta_2 q_n + \zeta_3 \right)$$
$$\zeta_1 = -2.2 \cdot T_n^2 + 3.7 \cdot T_n - 1.6,$$
$$\zeta_2 = 18.9 \cdot T_n^2 - 32.4 \cdot T_n + 14.2,$$
$$\zeta_3 = -19.8 \cdot T_n^2 + 35.8 \cdot T_n - 15.8,$$

and

$$\chi(T_o) = X(T_o) / X(T_{o,0}),$$
$$X(T_o) = \exp\left[(-60.24 + 31.15/T_n + 23.36 \cdot \ln(3T_n) \right].$$

Here $\zeta_\star = 10$, $q_n = q/290$ ppmv, $T_n = T_o/300$ K, T_o stands for globally averaged annual mean sea surface temperature. The term $T_{n,0}$ is defined in the same way as T_n, but with the initial value $T_{o,0}$ for the globally averaged annual mean sea surface temperature. In turn,

$$\frac{dD}{dt} = F_o. \quad (2)$$

With the IAP RAS CM, a CMIP5 (Coupled Models Intercomparison Project, phase 5 Taylor et al., 2012) 'historic' simulation for 1700–2005, continued by a RCP 2.6 (Representative Concentration Pathway 2.6) simulation for 2006–2300, was performed. Both parts of the run were forced by the fossil fuels emissions of carbon dioxide into the atmosphere, by the atmospheric burdens of methane, nitrous peroxide, and tropospheric sulfate aerosols, by the total solar irradiance (TSI), by extent of crops and pastures (affecting both surface albedo and CO_2 land use emissions into the atmosphere), and by the optical depth of stratospheric aerosol (associated with volcanic eruptions). The simulation was similar to that reported by Eliseev et al. (2014b) but uses a model version with a modified scheme for natural fires. The latter modification does not markedly affect global mean temperature and the atmospheric CO_2 carbon content. We chose scenario RCP 2.6 among other RCP scenarios because it is the most interesting for the problem at hand: in this scenario the atmospheric CO_2 content peaks in the middle of the 21st century and declines thereafter.

We found that even the apparent lag between the global mean temperature T and the atmospheric CO_2 carbon content q depends on time interval. When anthropogenic carbon dioxide emissions into the atmosphere are relatively small, changes in T and q in our model are caused by either volcanic activity or changes in total solar irradiance (internal climate variability is rather small in our model

as well as in many other contemporary EMICs (Eby et al., 2013)). For instance, in 1815 A.D., the Earth climate was disturbed by the eruption of Tambora, which was the strongest eruption during the last several centuries. In response to this eruption (and the unknown 1809 A.D. eruption), in our model T dropped by about 1 °C within two years after this eruption (Fig. 2a). This response is similar to that obtained from proxy data and from simulations with other climate models (for overview, see Raible et al., 2016). In turn, q decreased by 7 ppmv to 1822 A.D. Such excursion of q aftermath of this eruption is not visible in the borehole CO_2 content data, which is likely due to insufficient time resolution of these data (Raible et al., 2016). We note that the response of q, which is similar to ours, was obtained by Kandlbauer et al. (2013) in their Tambora eruption simulations with HadGEM2-ES and by Frölicher et al. (2011) in their comparable Pin.5x simulation. In addition, strong, up to 15 ppmv, negative excursions of the atmospheric CO_2 content was simulated by Foley et al. (2014) with a suit of Earth system models as a response to the 1258 A.D. eruption which was even stronger than then Tambora one. Thus, for time interval with weak anthropogenic CO_2 emissions into the atmosphere and strong natural forcing, T leads q. This lag amounts for few years. During these time intervals, carbon fluxes from the atmosphere into the ocean, F_o, and into the terrestrial ecosystems (excluding land use emissions), F_l, have similar magnitudes to each other.

This is in contrast to the 21st century with the aforementioned peak in the atmospheric CO_2 content. In this time interval, the time instant when T reaches its maximum is delayed with respect to the corresponding time instant for q by about 10 yr (Fig. 2b). This exemplifies that even the sign of the lag between q and T depends on the type of the forcing. In this period, the F_o magnitude is several-fold larger than the magnitude of F_l.

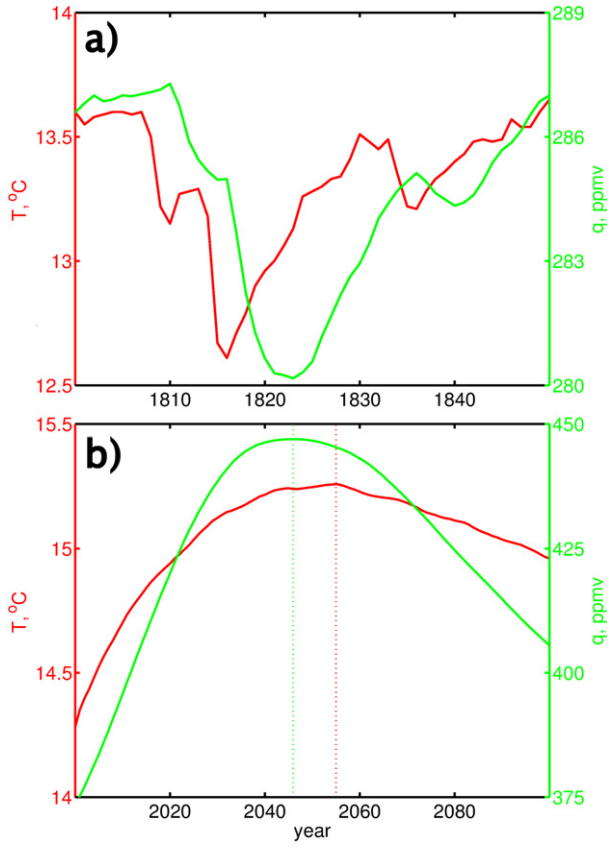

Fig. 2. Changes of the global mean temperature T (red) and the CO_2 atmospheric content (green) in the CMIP5 simulation with the IAP RAS CM for years 1800–1850 (a) and 2000–2100 (b). In the latter panel, the data are smoothed by the 11-year running means.

More formally magnitude of the lag between the global mean temperature and the atmospheric CO_2 content may be determined as a time lag at which the cross-correlation function between q and T has maximum (e.g., Mokhov et al. 2005a; Ganopolski and Roche, 2009; Humlum et al., 2013). In addition, the long- and short-term components of the response may be extracted by calculating the trends of q and T for a time interval under study. We use a quadratic polynomial function of time as a long-term response of our model and define the short-term response as a difference between the model-simulated time series of q and T and their long-term counterparts.

Thus computed lag, Δ, again depends on the studied time interval. For 1800–1850, both the raw data and the short-term component lead to $\Delta = 4$ yr. Here and below, we adopt a notation that $\Delta > 0$ ($\Delta < 0$) means that q lags T (q leads T). For the long-term component, Δ is close to zero for this time interval. For 2000–2100, the short-term Δ is positive (but very small) because of the 11-year solar cycle included in the RCP scenarios. In turn, the long-term Δ is equal to 8 yr. For 1950–2000, when both strong anthropogenic emissions of CO_2 into the atmosphere and volcanic + solar forcing are present, the short-term and the raw-data-calculated $\Delta = 3$ yr, while the long-term lag is uncertain because of absence of relevant extrema in q and T.

As a result, our model is capable to reproduce, at least qualitatively, the lag of q behind T at the interannual time scale (with caveats discussed in Discussions and conclusions). As it was hypothesized in the Introduction, the mutual lag between the global mean temperature and the atmospheric CO_2 content arises both because of the causal relationships in the Earth system and because of the inherent time scales in this system. To make both concepts more clear, idealized simulations with the IAP RAS CM were performed as well. These simulations are reported in the next section.

2.2. Simulations with periodic external forcings

The latter simulations are driven by the synthetic periodic forcings. The first simulation group is forced by the external non-greenhouse radiative forcing. For technical simplicity, we use TSI as a forcing agent. We note that our simulations are not aimed to represent any real TSI variability. We construct the TSI time series which vary as a sine function of time with period P and relative amplitude a_{TSI}. Depending on the ensemble member, period P is changed from 5 to 2000 yr, and relative amplitude is set either to 1% or to 2% of the present-day TSI value. Thereafter, this ensemble is referred to as TSIens.

The second simulation group, ECO2ens, is forced by the external carbon dioxide emissions E into the atmosphere. These emissions again follow the sine function of time with period P and absolute amplitude a_E. Depending on ensemble member, period P is varied from 5 to 2000 yr, and the amplitude a_E is changed from 1 to 10 PgC yr^{-1}.

The equilibrated preindustrial climate state is used as an initial condition for all simulations. All forcings, which are not described above explicitly, are set to the preindustrial values.

Our TSIens simulations are similar to those used by Willeit et al. (2014) with the Climber-2 and Climber-LPJ EMICs, both are driven by the periodic TSI forcing. Because the aim of the latter paper was to study the time scale dependence of the climate–carbon cycle feedback parameter, and taking into account that the atmospheric modules of the IAP RAS CM and Climber share similar approaches for description of atmospheric dynamics, our results might be considered as complementary to theirs.

Similar to that it was in the previous section, the lag Δ between T and q was determined via maximum cross-correlation function between these two variables.

These simulations show that sign of Δ depends on forcing type (Fig. 3). For ensemble ECO2ens, Δ is negative for all P and all a_E: q leads T. This lag monotonically increases with increasing P. It equals to few years at $P \leq 10$ yr and stabilizes at the value around 20 yr at $P \geq 100$ yr. The dependence on amplitude a_E is rather small.

For periods P up to few centuries, the most important contribution to the total carbon uptake $F_t = F_l + F_o$ is due to the terrestrial uptake which magnitude is larger than the magnitude of the oceanic counterpart by a factor of two. Oceanic and terrestrial carbon uptakes become comparable to each other at $P = 200$ yr. Terrestrial carbon uptake looses its importance at larger P, and for the millennium time scale $F_t \approx F_o$. Because at centennial time scale the lag between T and F_l is smaller than the lag between T and F_o, lag between T and q increases by magnitude at larger P as well. We note that increasing importance of the oceanic carbon with increasing time scale of external forcing is a rather trivial consequence of inertia of the oceanic DIC (below it is shown that the relaxation time scale of the combined Eqs. (1) and (2) is about of 100 yr).

More complex behavior is exhibited for ensemble TSIens. Temperature leads the atmospheric carbon dioxide content if $P \leq P_{cr} = 450$ yr and lags behind q otherwise. The former behavior is consistent with that expected for the radiatively forced system (Fig. 1b). The largest values of Δ, from 12 to 14 yr, are attained for forcing periods from 50 to 200 yr. In contrast to ECO2ens, Δ does not stabilize for forcing periods of the order of few centuries. For instance, $|\Delta|$ is large as 35 yr at $P = 1000$ yr, and it equals to 73 yr at $P = 2000$ yr. Again, the dependence on relative amplitude is small.

As it was for the ECO2ens numerical experiments, in the TSIens simulations, Δ depends on the contribution of oceanic carbon uptake in F_t. At centennial time scales, when $\Delta > 0$, $F_t \approx F_l$ (Fig 4a). Both uptakes are in approximate anti-phase with T. At this time scale, the maximum deviations of q and soil carbon stock M_s from their initial values are of similar magnitudes (if the former is expressed in mass units) while amplitudes of respective deviations of vegetation carbon stock M_v and the global stock of the dissolved inorganic carbon in the ocean D are several-fold smaller (Fig. 5a).

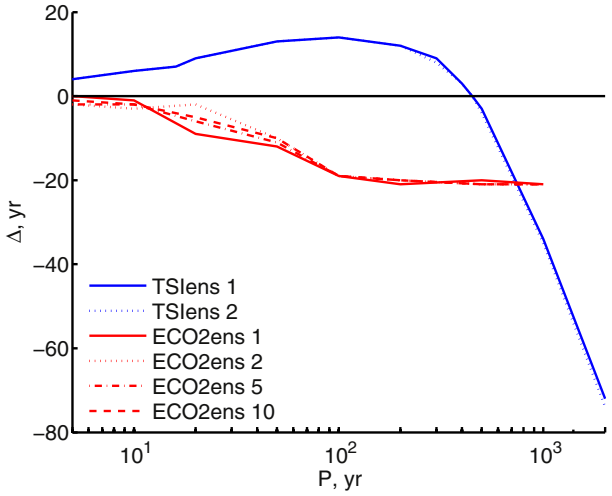

Fig. 3. Mutual lag between the global mean surface air temperature T and the atmospheric carbon dioxide content q in the IAP RAS CM simulations driven either by periodically varied total solar irradiance or by periodic CO_2 external emissions into the atmosphere (ensembles TSIens and ECO2ens respectively) with different amplitudes (shown by the numbers in legend). $\Delta > 0$ stands for q lagging behind T.

In contrast, both F_l and F_o make considerable contribution to total carbon uptake at millennium time scales (Fig 4b). As a result, the maximum deviation of D from its initial value becomes even larger than the corresponding deviation of q (again, if the latter is expressed in mass units) but smaller than the maximum respective deviation of M_s (Fig. 5b). The maximum deviation of M_v from its initial value is still several-fold smaller than the maximum deviations of other carbon stocks. We note that, at the millennium time scales, the atmospheric carbon content, terrestrial vegetation carbon stock, and oceanic DIC stock are approximately in phase with T and soil carbon stock is approximately anti-phase to all these variables.

Given the importance of oceanic carbon uptake in shaping Δ at sufficiently large P, we made additional TSIens simulations with the IAP RAS CM for forcing periods 200 yr, 450 yr, 500 yr, and 2000 yr. At each such simulation, either of two parameters, $\zeta_\star$ and $F_\star$, was changed. When $\zeta_\star$ is increased from 10 to 15 (decreased from 10 to 7), P_{cr} increases (decreases). By linear interpolation between simulations with different P, we estimate this increase (decrease) as amounting to 50 yr (36 yr). In turn, the increase (the decrease) of F_* from 2.5×10^{-2} PgC yr^{-1} ppmv^{-1} to 3×10^{-2} PgC yr^{-1} ppmv^{-1} (2×10^{-2} PgC yr^{-1} ppmv^{-1}) causes the decrease of P_{cr} on 38 yr (the increase of P_{cr} in 34 yr).

In addition, the just mentioned increase (decrease) of $\zeta_\star$ decreases (increases) the magnitude of Δ at $P = 2000$ yr to 37 yr (112 yr). The above-mentioned increase (decrease) of $F_\star$ changes the magnitude of Δ to 63 yr (85 yr).

2.3. Qualitative explanation of q leading T at centennial time scales in non-emission-forced runs

We note that $\Delta < 0$ for the TSIens simulations with $P > P_{cr}$ is not expected from the framework outlined in (Fig. 1b). However, it may be understood as a result of the climate–carbon cycle feedback taking into account that in the absence of external carbon emission into the atmosphere at each time instant t it is valid

$$q(t) + M(t) + D(t) = q(0) + M(0) + D(0) \quad (3)$$

(in this paragraph, we again express q in mass units to simplify notations; $M = M_v + M_s$). At first, change of temperature leads to change of soil carbon stock via change of heterotrophic respiration: if climate is cooled, M_s is increased, and if climate is warmed, soil carbon stock is depleted. If, say, CO_2 is released from the soil into the atmosphere, it starts to be taken up by the ocean. The latter process has a characteristic time scale $c_0/F_\star \sim 10^2$ yr, where $c_0 = 2.12$ PgC ppmv^{-1} is a conversion factor for q from the mixing ration units into the mass units. The time instant when M_s attains its extremum is slightly delayed with respect to the time instant when T extremum of the opposite sign is reached. In the IAP RAS CM, this delay amounts 37 yr for $P = 1000$ yr. Because changes of M_s dominate over M_v changes, M is also depletes under increasing temperature, while it increases under climate cooling. For sine changes of carbon stocks

$$M(t) = M(0) - M^{(0)}\sin(\omega t + \phi_{0,M}),$$
$$q(t) = q(0) + q^{(0)}\sin(\omega t + \phi_{0,q}),$$
$$D(t) = D(0) + D^{(0)}\sin(\omega t + \phi_{0,D}),$$

where $M^{(0)}$, $q^{(0)}$ and $D^{(0)}$ are amplitudes of changes of respective variables, $\phi_{0,M}$, $\phi_{0,q}$ and $\phi_{0,D}$ are their initial phases, and $\omega = 2\pi/P$. The signs in these equations are chosen to reflect the positive correlations between q and D and negative correlations between these two variables, on the one hand, and M, on the other. Without loss of

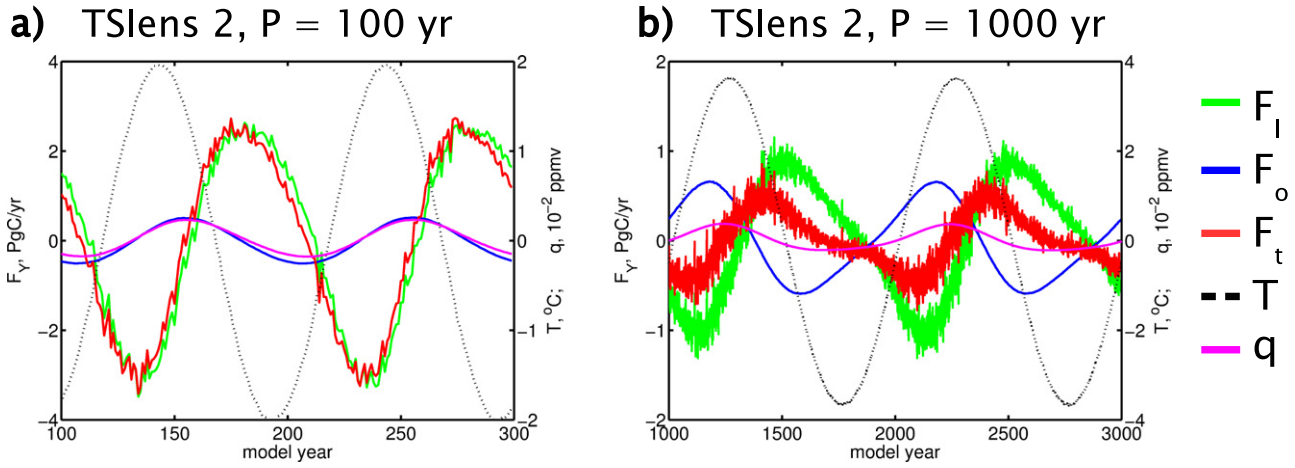

Fig. 4. Time series of the globally averaged annual mean surface air temperature T, atmospheric carbon dioxide content q (right ordinate axes are used for both variables) and total (subscript Y = t), terrestrial (Y = l), and oceanic (Y = o) carbon uptakes F_Y (left ordinate axes; F_Y is positive when it is directed from below into the atmosphere either to the ocean or to the terrestrial ecosystems) in the IAP RAS CM simulations TSIens 2 (see legend to Fig. 3). Initial values are removed from both T and q for plotting convenience. Only last 2 cycles of the simulations are shown.

generality one of initial phases (say, $\phi_{0,M}$) may be set equal to zero. Because Eq. (3) is valid at each time instant, one obtains

$$\sin\phi_{0,q} = -\frac{D^{(0)}}{q^{(0)}}\sin\phi_{0,D}. \tag{4}$$

The latter equation shows that sign of $\phi_{0,q}$ is opposite to the sign of $\phi_{0,D}$. Because D responds to changes in q, q should lead D (in our model, it could be directly obtained from Eqs. (1) and (2)), $\phi_{0,D} > 0$ (Fig. 5). Therefore, $\phi_{0,q} < 0$: q leads M. At millennium time scale the magnitudes of $q^{(0)}$ and $D^{(0)}$ are similar to each other. Thus, at this time scale the magnitude of $\phi_{0,q}$ should be similar to the magnitude of $\phi_{0,D}$. Because D is a rather inertial carbon stock, $\phi_{0,D} >$ is an equivalent of approximately of 100 yr. This value is sufficient to overcome the above-mentioned delay of M with respect to T and lead to q apparently leading T. This is in contrast to that occurring at centennial time scales, at which $D^{(0)}$ is several-fold smaller than $q^{(0)}$, (Fig. 5a), and, therefore, ϕ_q is not sufficiently large. We note, however, that the part of the TSIens curves in Fig. 3 with 100 yr ¡ P ¡ P_{cr}, when Δ decreases at increasing P, may be considered as a signature of increasing ϕ_q while this increase is not sufficient to overcome the delay of M with respect to T.

The above-mentioned impact of temperature changes on soil carbon stock and Eq. (4) are necessary ingredients for q leading T at millennium time scales in non-emission-forced runs. Eq. (4) may be interpreted as follows. In our model, there are three carbon stocks: an inertial stock D, a stock with a moderate inertia M and a fast-responding stock q. If the sum of these stocks is conserved, fast-responding stock should apparently lead the system to compensate the large variations of inertial stock and match the moderate-inertia stock. This qualitative explanation is rather general and is expected to be non-model-dependent.

The latter arguments might be even generalized to drop an assumption about the sine shape of $M(t)$, $D(t)$, and $q(t)$. Again, temperature changes lead to changes of the terrestrial carbon stock M with some delay, and the resulting excessive q is taken up either by the terrestrial vegetation or by the ocean (or deficit of q is compensated by carbon release from these reservoirs). At relative short (centennial) time scale $\max|D - D(0)| \ll \max|q - q(0)|$, and, thus,

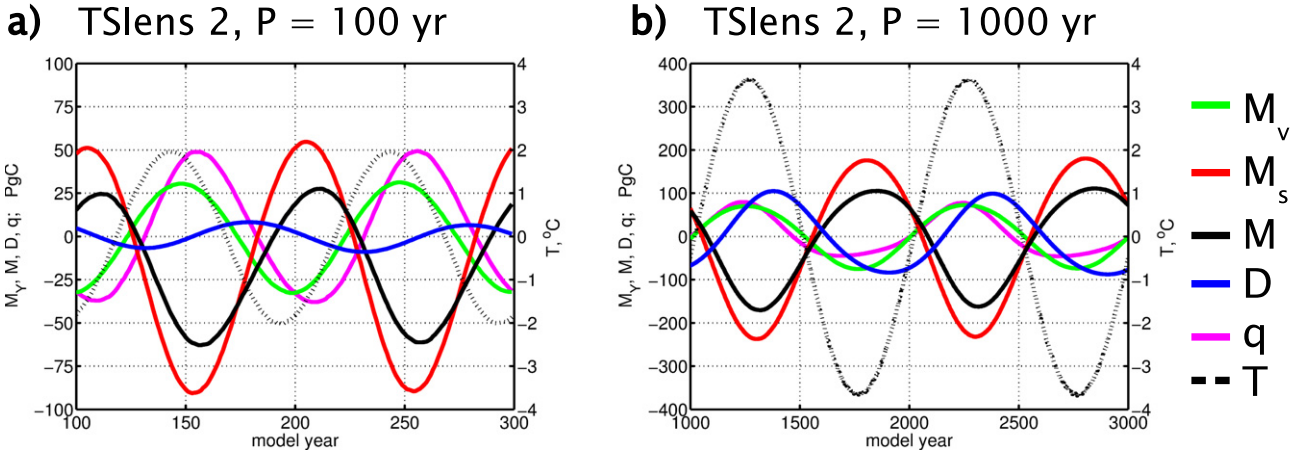

Fig. 5. Carbon stocks simulated by the IAP RAS CM in simulations TSIens 2 with periods 100 yr (a) and 1000 yr(b). Left ordinate axis: time series of the vegetation and soil carbon stocks (M_v and M_s correspondingly), total terrestrial ecosystem carbon stock $M = M_v + M_s$, atmospheric carbon dioxide content q (in mass units), and oceanic dissolved inorganic carbon stock D. Right ordinate axis: time series of the globally averaged annual mean surface air temperature T. Initial values are removed from all variables for plotting convenience. Only last 2 cycles of the simulations are shown.

$q(t)-q(0) \approx -(M(t)-M(0))$. Therefore, at this time scale, $q(t)$ together with $M(t)$ should lag behind T. At longer (millennium) time scales $\max|D-D(0)| \sim \max|q-q(0)|$, and, thus, $q(t)-q(0)$ is set as a balance between M and D (Fig. 6). If D is sufficiently large, which is true at sufficiently long time scales, q should compensate the delay of D behind M. The latter eventually leads to q leading T. We note that this reasoning is even applicable for non-periodic variations in the climate system.

3. Interpretation with a conceptual climate–carbon cycle model

In this section, the results reported in Section 2 are further interpreted with a conceptual, globally averaged climate–carbon cycle model (Muryshev et al., 2015). In this section, T and q are defined as anomalies from the initial equilibrated state.

The latter model consists of only two equations. The first equation is for the Earth system heat content (e.g., Andreae et al., 2005; Masters and Benestad, 2013):

$$C\frac{dT}{dt} = R - \lambda T, \tag{5}$$

where C is heat capacity per unit area, R is radiative forcing, and the term λT represents all climate feedbacks in a linear fashion. Coefficient λ is referred to as climate sensitivity parameter and is inversely proportional to the global mean surface air temperature change per unit forcing. The radiative forcing is subdivided into the CO_2-related and CO_2-unrelated parts, correspondingly:

$$R = R_{CO_2} + R_X. \tag{6}$$

Here the CO_2-related forcing is

$$R_{CO_2} = R_0 \ln\left(1 + \frac{q}{q_0}\right), \tag{7}$$

where q_0 is the initial value of the atmospheric CO_2 content. For the contemporary climate models, $R_0 = 5.3\ \mathrm{W\,m^{-2}}$, λ is from 0.6 to 1.6 $\mathrm{W\,m^{-2}\,K^{-1}}$ (Flato et al., 2013, Table 9.5) (in the standard setup of the conceptual model, $\lambda = 1\ \mathrm{W\,m^{-2}\,K^{-1}}$ corresponding to the equilibrium sensitivity of surface air temperature to the doubling of the carbon dioxide content in the atmosphere $\Delta T_{xx} = 3.7$ K. This value is a factor of 1.7 larger than that for the IAP RAS CM. However, we want our conceptual model to be representative for the whole ensemble of the contemporary Earth system models. This is the reason why we set λ equal to the value approximately in the middle of the above-mentioned range for the contemporary climate models. The Earth system heat capacity per unit area $C = 1\ \mathrm{GJ\,m^{-2}\,K^{-1}}$ (Andreae et al., 2005).

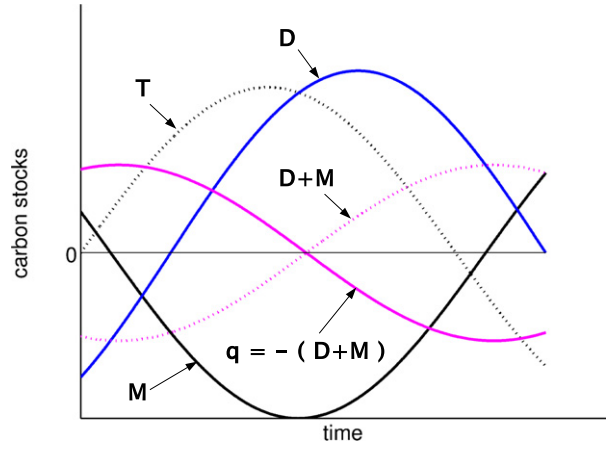

Fig. 6. A sketch of processes leading to T lagging behind q in the non-emission-forced scenarios.

The second equation represents the global carbon cycle:

$$c_0\frac{dq}{dt} = E - F_l - F_o, \tag{8}$$

where F_l and F_o are terrestrial and oceanic carbon uptakes. As before, E is external carbon emissions into the atmosphere. Thereafter we set $q_0 = 278$ ppmv.

Below we study different versions of Eqs. (5)–(8). These versions are obtained by different representations of F_l and F_o and by assumptions simplifying Eq. (7).

3.1. Numerical experiments with conceptual model

In this section, for terrestrial carbon uptake, we use the model (Eliseev and Mokhov, 2007; Lenton, 2000):

$$F_l = F_P - R_a - R_h, \tag{9}$$

where the gross photosynthesis, autotrophic respiration and heterotrophic respiration are, respectively:

$$\begin{aligned} F_P &= A_P g_f(q)\theta_P^{\vartheta}, \\ R_a &= A_a\,(M_v + M_{v,0})\,\theta_a^{\vartheta}, \\ R_h &= A_h\,(M_s + M_{s,0})\,\theta_h^{\vartheta}, \end{aligned} \tag{10}$$

where M_v and M_s are anomalies of the live vegetation and soil carbon stocks respectively, $M_{v,0}$ and $M_{s,0}$ are initial values of these stocks correspondingly, $A_P = 153.6\ \mathrm{PgC\,yr^{-1}}$, $A_a = 0.09\ \mathrm{yr^{-1}}$, $A_h = A_a M_{v,0}/M_{s,0}$ to ensure that in the steady state the terrestrial net primary production, NPP, which in this case is NPP $= F_P - R_a = R_h$, is approximately one half of F_P (Zhang et al., 2014), $\vartheta = T/T_0$, $T_0 = 1$ K, function

$$g_f(q) = \frac{q + q_0}{q + q_0 + q_{1/2}}$$

describes the photosynthesis response to the CO_2 enrichment of the atmosphere, $q_{1/2} = 318$ PgC, $\theta_P = 1.04$, $\theta_a = 1.08$, $\theta_h = 1.09$ (Lenton, 2000), and M_v and M_s are live vegetation and soil carbon stocks, correspondingly. The latter two variables obey the equations:

$$\begin{aligned} \frac{dM_v}{dt} &= P - R_a - L, \\ \frac{dM_s}{dt} &= L - R_h \end{aligned} \tag{11}$$

with the litter fall flux

$$L = A_L\,(M_v + M_{v,0})\,. \tag{12}$$

The litterfall coefficient $A_L = A_a$.

The oceanic carbon uptake is calculated by the same Bacastow-type model that was used as an oceanic carbon cycle module of IAP RAS CM (see Section 2.1) but with the globally and annually averaged surface (ocean + land) temperature in place of its sea surface counterpart as it is used in the IAP RAS CM. However, expressing T and q as anomalies leads to the replacement of $(q - q_0)$ in Eq. (1) by q. The globally averaged temperature T is used in equations for ζ and χ in place of T_o.

Because of difference in the terrestrial carbon cycle compartment from that implemented into the IAP RAS CM, the oceanic carbon cycle

is needed to be retuned. This was done by forcing the coupled conceptual model by the CMIP5 anthropogenic CO_2 emissions (http://cmip-pcmdi.llnl.gov/cmip5/forcing.html) for 1765–2005 and constraining the simulations to be consistent with the observed temperature trends during the 20th century as derived from the HadCRUT4 data (Morice et al., 2012), by the CMIP5 historical build-up of the atmospheric CO_2 content in 1765–2005, and by the estimates of the oceanic and terrestrial carbon uptakes as reported by Ciais et al. (2013, their Table 6.1). This procedure leaded to the value $F_\star = 3.5 \times 10^{-2}$ PgC yr^{-1} ppmv^{-1} with the allowable range from 2.5×10^{-2} to 4.5×10^{-2} PgC yr^{-1} ppmv^{-1}.

With this model, the simulations is performed similar to those described in Section 2. At first, the model is forced by the CMIP5-like forcings in three combinations: i) solar and volcanic forcings, ii) anthropogenic (both fossil fuel burning and land use) emissions of CO_2 into the atmosphere, and iii) combination of items i and ii. The results of these simulations are similar to those obtained in Section 2.1, but with somewhat increased lags (not shown). This is true for both lags Δ based on cross-correlation function and visual delays (similar to those shown in Fig. 2).

Then, we performed the simulations with periodically-varying forcing. One group of such simulations is the numerical experiments driven by the external CO_2 emissions (ensemble ECO2ens). Another group is the simulations RFens with periodically-varied radiative forcing R_X of unspecified origin. In different members of both latter ensembles, the period of the forcing is changed from 1 to 10,000 yr.

This model is able to qualitatively simulate mutual lags between T and q depending on the type of the forcing obtained with an EMIC. In particular, Δ is negative (q leads T) for the ECO2ens runs. Similar to that for the IAP RAS CM, this lag increases with increasing P and has an asymptote with the value of 32 yr (Fig. 7). We made additional simulations with our numerical conceptual model by changing values of λ. In these simulations, the asymptotic value of Δ is inversely proportional to λ (i.e., proportional to ΔT_{xx}). This asymptotic value increases to 40 yr at $\lambda = 0.8$ W m^{-2} K^{-1} and decreases to 18 yr at $\lambda = 1.8$ W m^{-2} K^{-1} (recall that the default value of this parameter in our conceptual model is $\lambda = 1$ W m^{-2} K^{-1}).

In turn, $\Delta > 0$ if $P \le 320$ yr in the RFens simulations with a nonlinear conceptual model (q lags behind T). This value of P_{cr} is of the same order of magnitude as it was obtained in simulations TSIens with our EMIC. Maximum $\Delta = 10$ yr, is reached at P which is between 100 and 150 yr. This is similar to the results obtained with an EMIC in Section 2.2. For larger periods, $\Delta < 0$ (q leads T) which corresponds to the results reported in Section 2.2. Because the studied range of P is wider in the simulations RFens with a conceptual model with respect to the EMIC simulations TSIens, in the former numerical experiments Δ eventually approaches the asymptotic value 75 yr at P slightly below 10^4 yr. $F_\star$ is increased from the default value 3.5×10^{-2} PgC yr^{-1} ppmv^{-1} to 4.5×10^{-2} PgC yr^{-1} ppmv^{-1}, this asymptotic value is decreased to 53 yr, and when $F_\star$ is decreased to 2.5×10^{-2} PgC yr^{-1} ppmv^{-1}, it is increased to 116 yr. While this asymptotic value is potentially interesting and its value depends on the governing parameters of the model (e.g., Fig. 7), an analysis of this asymptotic value is not pursued in this paper further because it is likely that this value is affected by the longer-term processes which are neglected in our models (see Discussions and conclusions)

In additional simulations, in which parameters of both oceanic ($F_\star$ and $\zeta_\star$) and terrestrial (A_h) carbon cycles are changed from their default (indicated above) values, we found that the value P_{cr}, is negative monotonic with respect to $F_\star$ and positive monotonic with respect to $\zeta_\star$ (Figs. 7 and 8). This is qualitatively similar to that obtained with the IAP RAS CM. For instance, when $F_\star$ is increased from the default value 3.5×10^{-2} PgC yr^{-1} ppmv^{-1} to 4.5×10^{-2} PgC yr^{-1} ppmv^{-1}, P_{cr} in the conceptual model decreases to 300 yr, and when $F_\star$ is decreased to 2.5×10^{-2} PgC yr^{-1} ppmv^{-1}, P_{cr} in increases to 360 yr. In addition, this critical period positive monotonic with respect to A_h.

The behavior of carbon uptakes and stocks in this conceptual model is similar to that exhibited for the IAP RAS CM at the same time scale (cf. Fig. 9 with Fig. 4, and Fig. 10 with Fig. 5). At centennial time scale, total carbon uptake F_t is determined mainly by the terrestrial carbon uptake irrespective of the type of the forcing. Similar to that it was for the IAP RAS CM, an importance of the oceanic carbon uptake increases in the conceptual model in the radiatively forced simulations at millennium time scale. The relative importance of different carbon stocks at a given time scale in the conceptual model is similar to that exhibited for the IAP RAS CM. We note, however, that the precise values of maximum deviations of carbon stocks in the conceptual model differ from their IAP RAS CM counterparts because of the different climate sensitivities between these two models and different terrestrial carbon cycles schemes implemented in these models. The latter leads to different temperature sensitivities of terrestrial (and, because of the retuning, oceanic) carbon uptakes between the IAP RAS CM and the conceptual model:

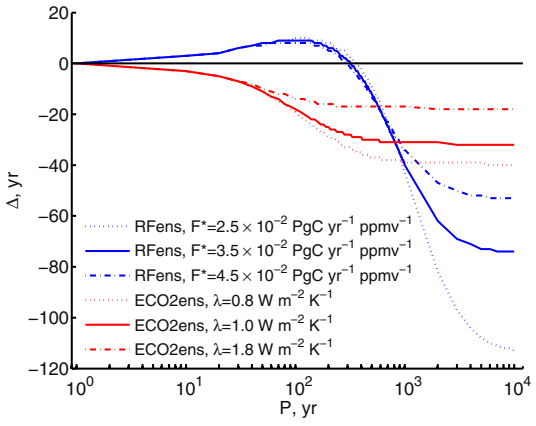

Fig. 7. Mutual lag between the global mean surface air temperature T and the atmospheric carbon dioxide content q in the numerical experiments with a conceptual climate–carbon cycle model driven either by ghost radiative forcing or by periodic CO_2 external emissions into the atmosphere. $\Delta > 0$ stands for q lagging behind T. Calculations are performed with model versions with different values of the oceanic uptake scaling factor $F_\star$ and climate sensitivity λ.

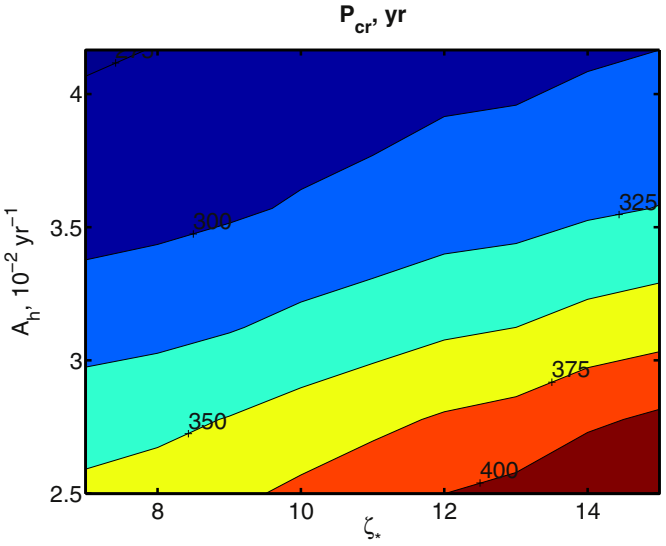

Fig. 8. Dependence of P_{cr} in the simulations with the nonlinear conceptual model on evasion factor coefficient $\zeta_\star$ (abscissas) and the heterotrophic respiration coefficient A_h (ordinates).

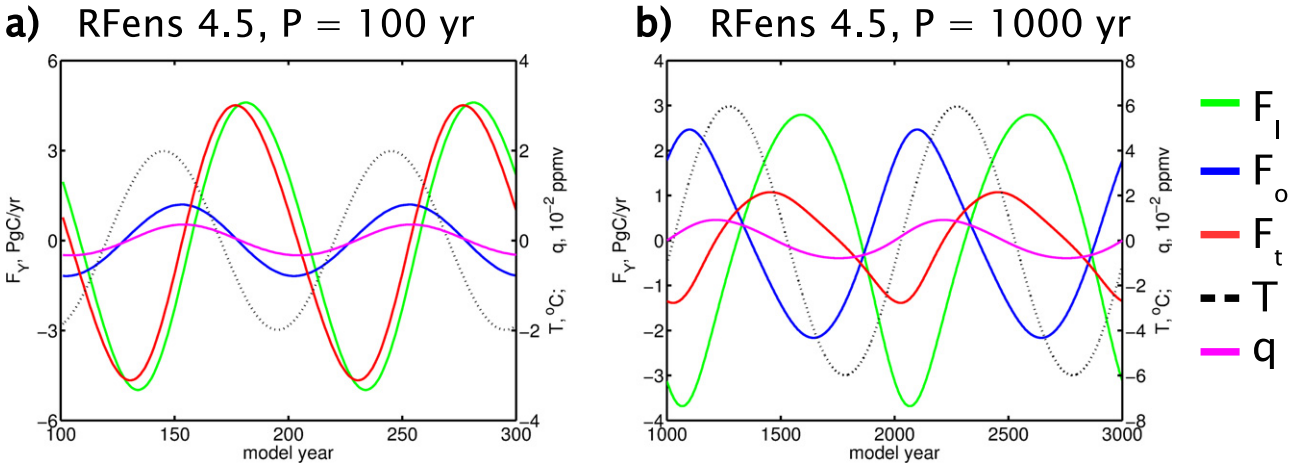

Fig. 9. Similar to Fig. 4, but for the nonlinear conceptual model. Shown are simulations RFens with the specified radiative forcing amplitude 4.5 W m^{-2} (corresponding to the TSIens 2 simulations).

in general, these uptakes are more sensitive to temperature changes in the conceptual model than in the IAP RAS CM (compare Figs. 4 and 9).

As a whole, the RFens simulations with this conceptual model may be used to interpret $\Delta < 0$ for the IAP RAS CM simulations TSIens, and the ECO2ens simulations with the conceptual model may be used to interpret their IAP RAS CM counterpart. This goal will be pursued in Section 3.2.

3.2. Linear conceptual model

The conceptual model, used in the previous subsection, is further simplified to obtain closed-form solutions. At first, in Eq. (7) the logarithm is replaced by a linear function corresponding to the leading term of the respective Taylor expansion (assuming that $|q| < q_0$):

$$R_{CO_2} = R_0 \frac{q}{q_0}. \tag{13}$$

Next, the terrestrial and oceanic carbon uptakes are represented by the sums of terms, proportional either to q or to T (Boer and Arora, 2013):

$$\begin{aligned} F_l &= -B_l q - \Gamma_l T, \\ F_o &= -B_o q - \Gamma_o T. \end{aligned} \tag{14}$$

Here the coefficients B_l and B_o represent the direct effects of the CO_2 build up in the atmosphere on the oceanic and terrestrial carbon uptakes (carbon-concentration feedback) (Ciais et al., 2013). In turn, Γ_l and Γ_o are coefficients of climate–carbon feedback (Ciais et al., 2013) and represent all impact of climate changes on carbon fluxes from the atmosphere into the ocean an terrestrial ecosystems. For sign convention as in Eq. (14), all contemporary Earth system models has $B_l < 0$, $B_o < 0$, $\Gamma_l > 0$, and $\Gamma_o > 0$ (Friedlingstein et al., 2006; Eliseev and Mokhov, 2011; Arora et al., 2013; Ciais et al., 2013). We note that our sign convention for B_Y and Γ_Y ($Y = l, o$) is inverse to that commonly used (Ciais et al., 2013), but preserved in the present paper for technical convenience.

Ignoring transients, the closed-form solutions of the linearized system for all types of periodic external forcings are sought in the form

$$\begin{aligned} q(t) &= q^{(0)} \sin\left(\omega\left(t + t_{0,q}\right)\right) = q_s \sin \omega t + q_c \cos \omega t, \\ T(t) &= T^{(0)} \sin\left(\omega\left(t + t_{0,T}\right)\right) = T_s \sin \omega t + T_c \cos \omega t. \end{aligned} \tag{15}$$

Here $q^{(0)}$ and $T^{(0)}$ are amplitudes, $\omega = 2\pi/P$, and $\phi_{0,q} = \omega t_{0,q}$ and $\phi_{0,T} = \omega t_{0,T}$ are initial phases of $q(t)$ and $T(t)$ respectively. In this set-up, the mutual lag between these two variables is $t_{0,T} - t_{0,q}$ with the same sign assignment as above.

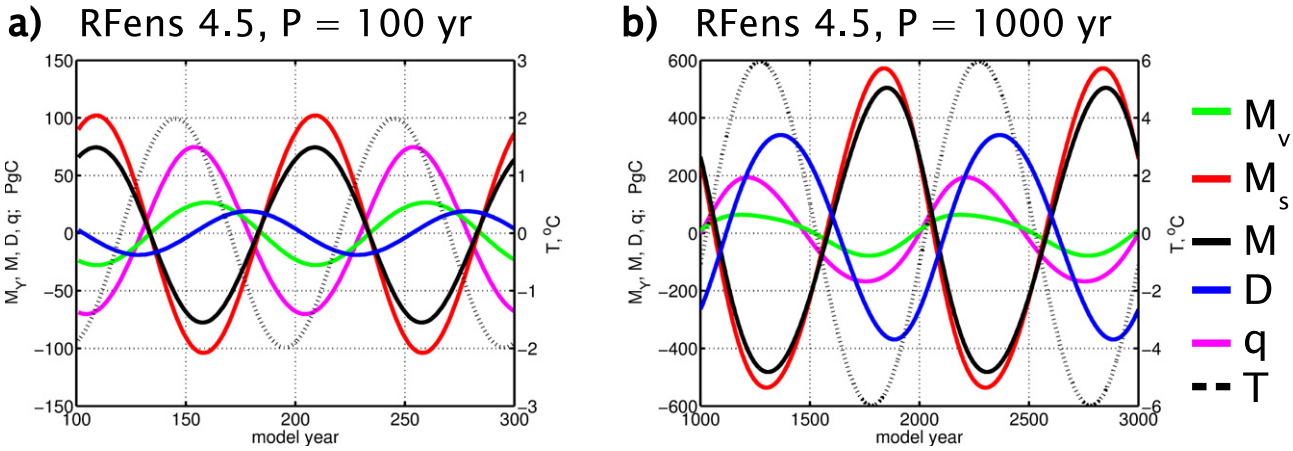

Fig. 10. Similar to Fig. 5 but for the nonlinear conceptual model simulations RFens with the specified radiative forcing amplitude 4.5 W m^{-2}.

At first, consider the case $E(t) \equiv 0$, $R(t) \neq 0$. One obtains

$$\begin{aligned}
\sin\phi_{0,T} &= -\frac{a_1}{\left(a_1^2 + a_2^2\right)^{1/2}},\\
\cos\phi_{0,T} &= -\frac{a_2}{\left(a_1^2 + a_2^2\right)^{1/2}},\\
\sin\phi_{0,q} &= \sin\phi_{0,T} \cdot \frac{\omega\frac{a_2}{a_1} + B}{\left(\omega^2 + \beta^2\right)^{1/2}}\\
\cos\phi_{0,q} &= \cos\phi_{0,T} \cdot \frac{\omega\frac{a_1}{a_2} - B}{\left(\omega^2 + B^2\right)^{1/2}}.
\end{aligned} \tag{16}$$

Here,

$$\begin{aligned}
B &= B_\mathrm{l} + B_\mathrm{o},\\
a_1 &= \omega\left(1 + \frac{r\Gamma}{\omega^2 + B^2}\right),\\
a_2 &= \nu - \frac{rB\Gamma}{\omega^2 + B^2},\\
\Gamma &= \Gamma_\mathrm{l} + \Gamma_\mathrm{o},\\
\nu &= -\lambda/C,\\
r &= R_0/(Cq_0).
\end{aligned}$$

For $B < 0$ and $\nu < 0$, one sees

$$E(t) \equiv 0, R(t) \neq 0: \begin{cases} t_{0,T} - t_{0,q} > 0 & \text{if } \Gamma > 0 \quad \Rightarrow \quad T \text{ leads } q,\\ t_{0,T} - t_{0,q} < 0 & \text{if } \Gamma < 0 \quad \Rightarrow \quad q \text{ leads } T. \end{cases} \tag{17}$$

In our sign convention, $\Gamma > 0$ corresponds to the case when the terrestrial carbon uptake is suppressed at higher temperatures, which corresponds to the positive climate–carbon cycle feedback. This sign of Γ is characteristic for all contemporary Earth system models near the present-day climate state (see above). Thus, it is revealed that q lagging behind T under external radiative forcing (and when the external CO_2 emissions are absent) is due to the climate–carbon feedback.

The case $E(t) \neq 0$, $R(t) \equiv 0$ may be studied in a way similar to that just figured. The system Eqs. (5)–(8), linearized according to Eqs. (13)–(14), is not changed qualitatively if q and T are interchanged. However, because in this case r and γ are interchanged as well, and r is always positive, one sees

$$E(t) \neq 0, R(t) \equiv 0: \qquad t_{0,T} - t_{0,q} < 0 \qquad \Rightarrow \qquad q \text{ leads } T. \tag{18}$$

Lag in Eq. (18) arises owing to non-zero r associated with greenhouse radiative forcing and thermal inertia of the Earth system.

It could be shown from this linearized model, that the asymptotic (achieved at infinitely large P) value of Δ is $|\nu|^{-1} = C/\lambda$. This dependence of asymptotic Δ on λ is the same that was exhibited for the nonlinear conceptual model in previous section. This values are in close agreements with the asymptotic values of $|Delta$ in the ECO2ens runs as obtained from the conceptual model runs with different values of λ.

As a result, this linear model supports both the general framework outlined in Fig. 1 and, partly, the numerical experiments with our EMIC (Section 2.2) and with an original conceptual model (Section 3.1). However, for this linear model, $\Delta < 0$ at time scales from several centuries to several tens of millennia remains unexplained. The latter will be studied in the next section.

3.3. A conceptual model for q leading T at time scales of the order of several centuries in the non-emission-forced runs

In this section, we further simplify our linear conceptual model. At first, we consider temperature variations as given in the form

$$T(t) = T^{(0)} \sin\omega t. \tag{19}$$

The latter implies that $t_{0,T} = 0$. In contrast to the previous section, we calculate the terrestrial and oceanic carbon uptakes via equations obtained via formal linearization of Eqs. (1)–(12):

$$\begin{aligned}
F_\mathrm{l} &= -\beta_\mathrm{l} q - \gamma_\mathrm{l} T - A_\mathrm{a} M,\\
F_\mathrm{o} &= -\beta_\mathrm{o} q - \alpha D.
\end{aligned} \tag{20}$$

Here

$$\begin{aligned}
M &= M_\mathrm{v} + M_\mathrm{s},\\
\beta_\mathrm{l} &= -A_\mathrm{P}\left.\frac{dg_\mathrm{f}}{dq}\right|_{q=0},\\
\gamma_\mathrm{l} &= -\left[A_\mathrm{P} g_\mathrm{f}|_{q=0}\left(\theta_\mathrm{P} - 1\right) + A_M\left(\theta_\mathrm{a} + \theta_\mathrm{h} - 2\right)\right] T_0^{-1},\\
\beta_\mathrm{o} &= -\frac{F_*}{c_0},\\
\alpha &= F_* \cdot \zeta|_{T=0,\ q=0} \cdot \frac{q_0}{D_0}.
\end{aligned}$$

The value of the effective coefficient of the ecosystem (autotrophic + heterotrophic) respiration A_M should lie between A_a and A_h. Strict but awkward formula for A_M could be obtained, but here, for simplicity, and because the soil carbon stock is much more important for the problem at hand than the vegetation one (Sections 2.2 and 3.1), we just set A_M equal to A_h. The temperature dependent term in Eq. (20) enters F_l but not F_o. This term in F_o formally belongs to the second-order terms and is dropped for this reason. The latter agrees with a common feature of the contemporary climate–carbon cycle models that the oceanic contribution to the carbon–climate feedback, associated with this term (Friedlingstein et al., 2003; Arora et al., 2013), is small relative to the respective contribution of terrestrial ecosystems (Friedlingstein et al., 2006; Arora et al., 2013). We note, however, that the additional term in the oceanic uptake, αD, which is absent in convenient technics to study the climate–carbon feedback, enters Eq. (20). This term represents the feedback of the DIC content in the ocean on F_o. We note that the resulting equations observe the necessary ingredients to get the sign change of Δ in such experiments: temperature-forced change of the terrestrial carbon stock M, compensation of this change by the oceanic uptake or outgassing, and the delayed change of D with respect to change of M. The conservation equation $c_0 q + M + D = 0$ is explicitly used.

Consider only the case $E(t) \equiv 0$, $R(t) \neq 0$. Because our goal in this section is just to explain the change of sign of Δ, we do not show a closed form solution of the linearized carbon budget equation subject to Eq. (19). Instead, we note that $\Delta = 0$ for solutions of the form (15) corresponds to $q_\mathrm{c} = 0$. Thus, the frequency at which Δ changes sign may be found as

$$\omega_\mathrm{cr} = \left[\beta_\mathrm{o}(\alpha - A_M) - \alpha^2\right]^{1/2}. \tag{21}$$

For ζ from 9 to 15 (Maier-Reimer and Hasselmann, 1987) and the above-listed values of other parameters, the sign change occurs at $\omega_\mathrm{cr} \leq 2.2 \times 10^{-2}\mathrm{yr}^{-1}$ which corresponds to the forcing period $P_\mathrm{cr} \geq 2.9 \times 10^2$ yr (Fig. 8). For the central values of parameters, $P_\mathrm{cr} = 330$ yr. This value with a good agreement with the value obtained in numerical simulations. We note that ω_cr exists only if α

is small enough. Moreover, for realistic values of parameters, Eq. (21) shows the same parametric sensitivity of P_{cr} with respect to $\zeta|_{T=0,\,q=0}$ (positive monotonic) and $F_\star$ (negative monotonic; this is obvious from Eq. (21)). In addition, P_{cr} is negative monotonic with respect to A_M. This behavior is similar to that exhibited in the numerical periodically-forced non-emission simulations presented in Fig. 8.

4. Discussions and conclusions

In this paper, we have extended the results reported by Muryshev et al. (2015) where it was shown that mutual lags between the global temperature T and the atmospheric carbon dioxide content q depend on the type of the forcing and on its time scale. We used an EMIC as a basis for our results and used a conceptual model to interpret the results obtained with an EMIC. We note that similar ideas were implicit in Masters and Benestad (2013) as well.

In agreement with our initial idea, T lags behind q when the Earth system dynamics is caused by anthropogenic emissions of carbon dioxide into the atmosphere. The latter occurs irrespectively of the forcing time scale. In turn, non-greenhouse radiative forcing results in T leading q if the forcing time scale is not larger than few centuries.

However, contrary to the initial idea, the global mean surface air temperature lags behind the atmospheric CO_2 content if the model is driven by non-greenhouse radiative forcing and provided that the forcing time scale is larger than 4×10^2 yr. The latter is a prominent example that lagged correlation does not necessarily represent causal relationships in a system: in such simulations, the applied forcing directly affects only the physical part of the Earth system, but q still leads T.

This apparently counter-intuitive result, however, is a direct consequence of i) temperature sensitivity of the soil carbon stock (which decreases if climate is warmed and increases if climate is cooled) and ii) conservation of total mass of carbon in the system if external carbon emissions are absent (fast-responding carbon stock q should lead the system to compensate inertial stock of oceanic DIC and fulfill this conservation of carbon mass), iii) oceanic branch of the carbon cycle becomes more important at longer time scales. This qualitative explanation is rather general. Thus, it is not expected to be model-dependent.

Our study contains a number of important caveats.

The first caveat is due to our neglect of carbonate dissolution in the ocean, which becomes important at time scales $\geq 5 \times 10^3$ yr (Archer et al., 2004). Its effect might be understood by decreasing α at such time scales. Because in our analysis its precise value is important only for existence and estimate of P_{cr}, which realistic value is of the order of several centuries, this caveat is presumably is not important for the results obtained in the present paper. We acknowledge, however, that carbonate dissolution is neglected in the IAP RAS CM as well, and its effect on the obtained results deserves further assessment.

Our model also neglects the igneous rocks weathering which becomes important at time scales of several millennia or longer (Archer et al., 2004; Archer and Brovkin, 2008; Zeebe, 2012). Implementation of weathering into the model would also affect the obtained results at such time scales.

Another potentially important caveat is due to neglect of possible changes of the intensity of the oceanic thermohaline circulation under climate change. This intensity could change either because of additional freshwater input or due to thermal forcing. This intensity may change either because of iceberg freshwater input from melting ice sheets during deglaciation (Schmittner and Galbraith, 2008; Ganopolski and Roche, 2009; Bouttes et al., 2012; Shakun et al., 2012; Landais et al., 2013; Zeebe, 2012) or due to variations in the wind-induced ventilation of the Southern Ocean (Anderson et al., 2009; Sigman et al., 2010; Skinner et al., 2010). Again, this effect can only be studied with more elaborated models than those used in the present paper.

Further, none of the models used in the present paper takes into account the humification of carbon in the soil. This process stores carbon in a very inert soil pool with a turnaround time which may be as large as $\sim 10^4$ yr (Brovkin et al., 2008) providing another large time scale which might affect mutual lags between q and T.

Finally, both our models lack realistic interannual variability. In the context of the present paper, this variability is likely to be qualitatively similar to non-greenhouse radiative forcing at the interannual to centennial time scales. It is expected to result in T leading q. We acknowledge that this topic deserves further study. This study, for instance, may be performed with the CMIP5 Earth system models using the technics based on that developed in Section 2.1.

All these caveats preclude to pursue the goals of our paper at time scales larger than several (or even few) millennia. This is the reason why we cut the simulations with a conceptual model at the forcing period of 10,100 yr. In addition, we note that our models lack ice-sheet dynamics which again has a response time scale of several millennia (Robinson et al., 2012).

Because all these caveats are most important at multi-millennium time scales, we believe that our results are able to explain, the mutual lags between q and T, at least for time scales up to few millennia. The basis of this belief is that the most important aspect, affecting the sign of mutual delay between these variables, is the part of the system (either climate or carbon cycle) which is directly affected by a given external forcing and the forcing time scale.

Acknowledgments

This work was supported by the Government of the Russian Federation (agreement no. 14.Z50.31.0033 with the Institute of Applied Physics RAS), by the Programs of the Russian Academy of Sciences, (project 0150-2015-0036) and by the Russian Foundation for Basic Research (grant 14-05-00639).

References

Anderson, R., Ali, S., Bradtmiller, L., Nielsen, S., Fleisher, M., Anderson, B., Burckle, L., 2009. Wind-driven upwelling in the Southern Ocean and the deglacial rise in atmospheric CO_2. Science 323 (5920), 1443–1448.

Andreae, M., Jones, C., Cox, P., 2005. Strong present-day aerosol cooling implies a hot future. Nature 435 (7046), 1187–1190.

Archer, D., Brovkin, V., 2008. The millennial atmospheric lifetime of anthropogenic CO_2. Clim. Change 90 (3), 283–297.

Archer, D., Martin, P., Buffett, B., Brovkin, V., Rahmstorf, S., Ganopolski, A., 2004. The importance of ocean temperature to global biogeochemistry. Earth. Planet. Sci. Lett. 222 (2), 333–348.

Arora, V., Boer, G., Friedlingstein, P., Eby, M., Jones, C., Christian, J., Bonan, G., Bopp, L., Brovkin, V., Cadule, P., Hajima, T., Ilyina, T., Lindsay, K., Tjiputra, J., Wu, T., 2013. Carbon-concentration and carbon-climate feedbacks in CMIP5 Earth system models. J. Climate 26 (15), 5289–5314.

Bereiter, B., Lüthi, D., Siegrista, M., Schüpbach, S., Stocker, T., Fischer, H., 2012. Mode change of millennial CO_2 variability during the last glacial cycle associated with a bipolar marine carbon seesaw. Proc. Nat. Acad. Sci. 109 (25), 9755–9760.

Bindoff, N., Stott, P., AchutaRao, K., Allen, M., Gillett, N., Gutzler, D., Hansingo, K., Hegerl, G., Hu, Y., Jain, S., Mokhov, I., Overland, J., Perlwitz, J., Sebbari, R., Zhang, X., 2013. Detection and attribution of climate change: from global to regional. In: Stocker, T., Qin, D., Plattner, G.-K., Tignor, M., Allen, S., Boschung, J., Nauels, A., Xia, Y., Bex, V., Midgley, P. (Eds.), Climate Change 2013: The Physical Science Basis. Contribution of Working Group I to the Fifth Assessment Report of the Intergovernmental Panel on Climate Change. Cambridge University Press, Cambridge and New York, pp. 867–952.

Boer, G., Arora, V., 2013. Feedbacks in emission-driven and concentration-driven global carbon budgets. J. Climate 26 (10), 3326–3341.

Bouttes, N., Roche, D., Paillard, D., 2012. Systematic study of the impact of fresh water fluxes on the glacial carbon cycle. Clim. Past 8 (2), 589–607.

Brovkin, V., Cherkinsky, A., Goryachkin, S., 2008. Estimating soil carbon turnover using radiocarbon data: a case-study for European Russia. Ecol. Mod. 216 (2), 178–187.

Caillon, N., Severinghaus, J., Jouzel, J., Barnola, J.M., Kang, J., Lipenkov, V., 2003. Timing of atmospheric CO_2 and Antarctic temperature changes across Termination III. Science 299 (5613), 1728–1731.

Canty, T., Mascioli, N., Smarte, M., Salawitch, R., 2013. An empirical model of global climate – part 1: a critical evaluation of volcanic cooling. Atmos. Chem. Phys. 13 (8), 3997–4031.

Ciais, P., Sabine, C., Bala, G., Bopp, L., Brovkin, V., Canadell, J., Chhabra, A., DeFries, R., Galloway, J., Heimann, M., Jones, C., Le Quéré, C., Myneni, R., Piao, S., Thornton, P., 2013. Carbon and other biogeochemical cycles. In: Stocker, T., Qin, D., Plattner, G.-K., Tignor, M., Allen, S., Boschung, J., Nauels, A., Xia, Y., Bex, V., Midgley, P. (Eds.), Climate Change 2013: The Physical Science Basis. Contribution of Working Group I to the Fifth Assessment Report of the Intergovernmental Panel on Climate Change.. Cambridge University Press, Cambridge and New York, pp. 465–570.

Claussen, M., Mysak, L., Weaver, A., Crucifix, M., Fichefet, T., Loutre, M.F., Weber, S., Alcamo, J., Alexeev, V., Berger, A., Calov, R., Ganopolski, A., Goosse, H., Lohmann, G., Lunkeit, F., Mokhov, I., Petoukhov, V., Stone, P., Wang, Z., 2002. Earth system models of intermediate complexity: closing the gap in the spectrum of climate system models. Clim. Dyn. 18 (7), 579–586.

Eby, M., Weaver, A., Alexander, K., Zickfeld, K., Abe-Ouchi, A., Cimatoribus, A., Crespin, E., Drijfhout, S., Edwards, N., Eliseev, A., Feulner, G., Fichefet, T., Forest, C., Goosse, H., Holden, P., Joos, F., Kawamiya, M., Kicklighter, D., Kienert, H., Matsumoto, K., Mokhov, I., Monier, E., Olsen, S., Pedersen, J., Perrette, M., Philippon-Berthier, G., Ridgwell, A., Schlosser, A., Schneider von Deimling, T., Shaffer, G., Smith, R., Spahni, R., Sokolov, A., Steinacher, M., Tachiiri, K., Tokos, K., Yoshimori, M., Zeng, N., Zhao, F., 2013. Historical and idealized climate model experiments: an EMIC intercomparison. Clim. Past 9 (3), 1111–1140.

Eliseev, A., 2011. Estimation of changes in characteristics of the climate and carbon cycle in the 21st century accounting for the uncertainty of terrestrial biota parameter values. Izvestiya. Atmos. Ocean. Phys. 47 (2), 131–153.

Eliseev, A., 2012. Climate change mitigation via sulfate injection to the stratosphere: impact on the global carbon cycle and terrestrial biosphere. Atmos. Ocean. Optics 25 (6), 405–413.

Eliseev, A., 2015. Impact of tropospheric sulphate aerosols on the terrestrial carbon cycle. Glob. Planet. Change 124, 30–40.

Eliseev, A., Arzhanov, M., Demchenko, P., Mokhov, I., 2009. Changes in climatic characteristics of Northern Hemisphere extratropical land in the 21st century: assessments with the IAP RAS climate model. Izvestiya. Atmos. Ocean. Phys. 45 (3), 271–283.

Eliseev, A., Demchenko, P., Arzhanov, M., Mokhov, I., 2014a. Transient hysteresis of near-surface permafrost response to external forcing. Clim. Dyn 42 (5-6), 1203–1215.

Eliseev, A., Mokhov, I., 2007. Carbon cycle-climate feedback sensitivity to parameter changes of a zero-dimensional terrestrial carbon cycle scheme in a climate model of intermediate complexity. Theor. Appl. Climatol. 89 (1-2), 9–24.

Eliseev, A., Mokhov, I., 2011. Uncertainty of climate response to natural and anthropogenic forcings due to different land use scenarios. Adv. Atmos. Sci. 28 (5), 1215–1232.

Eliseev, A., Mokhov, I., Chernokulsky, A., 2014b. An ensemble approach to simulate CO_2 emissions from natural fires. Biogeosciences 11 (12), 3205–3223.

Eliseev, A., Mokhov, I., Chernokulsky, A., 2014c. Influence of ground and peat fires on CO_2 emissions into the atmosphere. Doklady Earth Sci 459 (2), 1565–1569.

Eliseev, A., Sergeev, D., 2014. Impact of subgrid scale vegetation heterogeneity on the simulation of carbon cycle characteristics. Izvestiya. Atmos. Ocean. Phys. 50 (3), 225–235.

Flato, G., Marotzke, J., Abiodun, B., Braconnot, P., Chou, S., Collins, W., Cox, P., Driouech, F., Emori, S., Eyring, V., Forest, C., Gleckler, P., Guilyardi, E., Jakob, C., Kattsov, V., Reason, C., Rummukainen, M., 2013. Evaluation of climate models. In: Stocker, T., Qin, D., Plattner, G.-K., Tignor, M., Allen, S., Boschung, J., Nauels, A., Xia, Y., Bex, V., Midgley, P. (Eds.), Climate Change 2013: The Physical Science Basis. Contribution of Working Group I to the Fifth Assessment Report of the Intergovernmental Panel on Climate Change.. Cambridge University Press, Cambridge and New York, pp. 659–740.

Foley, A., Willeit, M., Brovkin, V., Feulner, G., Friend, A., 2014. Quantifying the global carbon cycle response to volcanic stratospheric aerosol radiative forcing using Earth system models. J. Geophys. Res.: Atmospheres 119 (1), 101–111.

Friedlingstein, P., Cox, P., Betts, R., Bopp, L., von Bloh, W., Brovkin, V., Doney, S., Eby, M., Fung, I., Govindasamy, B., John, J., Jones, C., Joos, F., Kato, T., Kawamiya, M., Knorr, W., Lindsay, K., Matthews, H., Raddatz, T., Rayner, P., Reick, C., Roeckner, E., Schnitzler, K.G., Schnur, R., Strassmann, K., Weaver, A., Yoshikawa, C., Zeng, N., 2006. Climate-carbon cycle feedback analysis: results from the *C⁴MIP* model intercomparison. J. Climate 19 (22), 3337–3353.

Friedlingstein, P., Dufresne, J.L., Cox, P., Rayner, P., 2003. How positive is the feedback between climate change and the carbon cycle? Tellus B 55 (2), 692–700.

Frölicher, T., Joos, F., Raible, C., 2011. Sensitivity of atmospheric CO_2 and climate to explosive volcanic eruptions. Biogeosciences 8 (8), 2317–2339.

Ganopolski, A., Petoukhov, V., Rahmstorf, S., Brovkin, V., Claussen, M., Eliseev, A., Kubatzki, C., 2001. CLIMBER-2: a climate system model of intermediate complexity. Part II: model sensitivity. Clim. Dyn 17 (10), 735–751.

Ganopolski, A., Roche, D., 2009. On the nature of lead-lag relationships during glacial-interglacial climate transitions. Quat. Sci. Rev. 28 (27-28), 337–3361.

Hartmann, D., Klein Tank, A., Rusticucci, M., Alexander, L., Brönnimann, S., Charabi, Y., Dentener, F., Dlugokencky, E., Easterling, D., Kaplan, A., Soden, B., Thorne, P., Wild, M., Zhai, P., 2013. Observations: atmosphere and surface. In: Stocker, T., Qin, D., Plattner, G.-K., Tignor, M., Allen, S., Boschung, J., Nauels, A., Xia, Y., Bex, V., Midgley, P. (Eds.), Climate Change 2013: The Physical Science Basis. Contribution of Working Group I to the Fifth Assessment Report of the Intergovernmental Panel on Climate Change. Cambridge University Press, Cambridge and New York, pp. 159–254.

Hegerl, G., Hasselmann, K., Cubasch, U., Mitchell, J., Roeckner, E., Voss, R., Waszkewitz, J., 1997. Multi-fingerprint detection and attribution analysis of greenhouse gas, greenhouse gas-plus-aerosol and solar forced climate change. Clim. Dyn. 13, 613–634.

Humlum, O., Stordahl, K., Solheim, J.E., 2013. The phase relation between atmospheric carbon dioxide and global temperature. Glob. Planet. Change 100, 51–69.

Idso, S., 1998. CO_2-induced global warming: a skeptic's view of potential climate change. Clim. Res 10 (1), 69–82.

Jones, G., Stott, P., Christidis, N., 2013. Attribution of observed historical near-surface temperature variations to anthropogenic and natural causes using CMIP5 simulations. J. Geophys. Res.: Atmospheres 118 (10), 4001–4024.

Kandlbauer, J., Hopcroft, P., Valdes, P., Sparks, R., 2013. Climate and carbon cycle response to the 1815 Tambora volcanic eruption. J. Geophys. Res.: Atmospheres 118 (22), 12497–12507.

Kern, Z., Leuenberger, M., 2013. Comment on "The phase relation between atmospheric carbon dioxide and global temperature" Humlum et al. [glob. planet. change 100: 51-69.]: isotopes ignored. Glob. Planet. Change 109, 1–2.

Landais, A., Dreyfus, G., Capron, E., Jouzel, J., Masson-Delmotte, V., Roche, D.M., Prié, F., Caillon, N., Chappellaz, J., Leuenberger, M., Lourantou, A., Parrenin, F., Raynaud, D., Teste, G., 2013. Two-phase change in CO_2, Antarctic temperature and global climate during Termination II. Nature Geosci. 6 (12), 1062–1065.

Lean, J., Rind, D., 2008. How natural and anthropogenic influences alter global and regional surface temperatures: 1889 to 2006. Geophys. Res. Lett. 35 (18), L18701.

Lenton, T., 2000. Land and ocean carbon cycle feedback effects on global warming in a simple Earth system model. Tellus B 52 (5), 1159–1188.

Lindzen, R., 1990. Some coolness concerning global warming. Bull. Amer. Met. Soc. 71 (3), 288–299.

Maier-Reimer, E., Hasselmann, K., 1987. Transport and storage of CO_2 in the ocean – an inorganic ocean-circulation carbon cycle model. Clim. Dyn. 2 (2), 63–90.

Masters, T., Benestad, R., 2013. Comment on "The phase relation between atmospheric carbon dioxide and global temperature". Glob. Planet. Change 106, 141–142.

Mikšovský, J., Holtanová, E., Pišoft, P., 2016. Imprints of climate forcings in global gridded temperature data. Earth, Syst. Dyn. 7 (1), 231–249.

Millero, F., 1995. Thermodynamics of carbon dioxide system in the ocean. Geophys. Cosmophys. Acta 59 (4), 661–677.

Mokhov, I., Bezverkhny, V., Karpenko, A., 2005a. Diagnosis of relative variations in atmospheric greenhouse gas contents and temperature from Vostok Antarctic ice-core paleoreconstructions. Izvestiya. Atmos. Ocean. Phys 41 (5), 523–536.

Mokhov, I., Demchenko, P., Eliseev, A., Khon, V., Khvorostyanov, D., 2002. Estimation of global and regional climate changes during the 19th–21st centuries on the basis of the IAP RAS model with consideration for anthropogenic forcing. Izvestiya. Atmos. Ocean. Phys. 38 (5), 555–568.

Mokhov, I., Eliseev, A., 2012. Modeling of global climate variations in the 20th–23rd centuries with new RCP scenarios of anthropogenic forcing. Doklady Earth Sci. 443 (2), 532–536.

Mokhov, I., Eliseev, A., Demchenko, P., Khon, V., Akperov, M., Arzhanov, M., Karpenko, A., Tikhonov, V., Chernokulsky, A., Sigaeva, E., 2005b. Climate changes and their assessment based on the IAP RAS global model simulations. Doklady Earth Sci. 402 (4), 591–595.

Mokhov, I., Eliseev, A., Karpenko, A., 2008. Decadal-to-centennial scale climate-carbon cycle interactions from global climate models simulations forced by anthropogenic emissions. In: Peretz, L. (Ed.), Climate Change Research Trends. Nova Sci. Publ. Hauppauge, NY, pp. 217–241.

Mokhov, I., Smirnov, D., 2009. Empirical estimates of the influence of natural and anthropogenic factors on the global surface temperature. Doklady Earth Sci. 427 (1), 798–803.

Mokhov, I., Smirnov, D., Karpenko, A., 2012. Assessments of the relationship of changes of the global surface air temperature with different natural and anthropogenic factors based on observations. Doklady Earth Sci. 443 (1), 381–387.

Monnin, E., Indermühle, A., Dällenbach, A., Flückiger, J., Stauffer, B., Stocker, T., Raynaud, D., Barnola, J.M., 2001. Atmospheric CO_2 concentrations over the last glacial termination. Science 291 (5501), 112–114.

Morice, C., Kennedy, J., Rayner, N., Jones, P., 2012. Quantifying uncertainties in global and regional temperature change using an ensemble of observational estimates: the HadCRUT4 data set. J. Geophys. Res.: Atmospheres 117 (D8), D08101.

Muryshev, K., Eliseev, A., Mokhov, I., Timazhev, A., 2015. A lag between temperature and atmospheric CO_2 concentration based on a simple coupled model of climate and the carbon cycle. Doklady Earth Sci. 463 (2), 863–867.

Myhre, G., Shindell, D., Bréon, F.M., Collins, W., Fuglestvedt, J., Huang, J., Koch, D., Lamarque, J.F., Lee, D., Mendoza, B., Nakajima, T., Robock, A., Stephens, G., Takemura, T., Zhang, H., 2013. Anthropogenic and natural radiative forcing. In: Stocker, T., Qin, D., Plattner, G.-K., Tignor, M., Allen, S., Boschung, J., Nauels, A., Xia, Y., Bex, V., Midgley, P. (Eds.), Climate Change 2013: The Physical Science Basis. Contribution of Working Group I to the Fifth Assessment Report of the Intergovernmental Panel on Climate Change. Cambridge University Press, Cambridge and New York, pp. 659–740.

Petoukhov, V., Claussen, M., Berger, A., Crucifix, M., Eby, M., Eliseev, A., Fichefet, T., Ganopolski, A., Goosse, H., Kamenkovich, I., Mokhov, I., Montoya, M., Mysak, L., Sokolov, A., Stone, P., Wang, Z., Weaver, A., 2005. EMIC intercomparison project (EMIP-CO2): comparative analysis of EMIC simulations of current climate and equilibrium and transient responses to atmospheric CO_2 doubling. Clim. Dyn 25 (4), 363–385.

Petoukhov, V., Ganopolski, A., Brovkin, V., Claussen, M., Eliseev, A., Kubatzki, K., Rahmstorf, S., 2000. CLIMBER-2: a climate system model of intermediate

complexity. Part I: model description and performance for present climate. Clim. Dyn 16 (1), 1–17.
Petoukhov, V., Mokhov, I., Eliseev, A., Semenov, V., 1998. The IAP RAS Global Climate Model. Dialogue-MSU, Moscow.
Quinn, J., 2010. Global Warming. Geophysical Counterpoints to the Enhanced Greenhouse Theory. Dorrance Publ., Pittsburgh.
Raible, C., Brönnimann, S., Auchmann, R., Brohan, P., Frölicher, T., Graf, H.F., Jones, P., Luterbacher, J., Muthers, S., Neukom, R., Robock, A., Self, S., Sudrajat, A., Timmreck, C., Wegmann, M., 2016. Tambora 1815 as a test case for high impact volcanic eruptions: Earth system effects. Wiley Interdis. Rev.: Climate Change 7 (4), 569–589.
Ribes, A., Terray, L., 2013. Application of regularised optimal fingerprint analysis for attribution. Part II: application to global near-surface temperature. Clim. Dyn. 41 (11-12), 2837–2853.
Richardson, M., 2013. Comment on "The phase relation between atmospheric carbon dioxide and global temperature" by Humlum, Stordahl and Solheim. Glob. Planet. Change 107, 226–228.
Robinson, A., Calov, R., Ganopolski, A., 2012. Multistability and critical thresholds of the Greenland ice sheet. Nature Clim. Change 2 (6), 429–432.
Scafetta, N., 2012. Testing an astronomically based decadal-scale empirical harmonic climate model versus the general circulation climate models. J. Atmos. Solar.-Terr. Phys. 80, 124–137.
Schmittner, A., Galbraith, E., 2008. Glacial greenhouse-gas fluctuations controlled by ocean circulation changes. Nature 456 (7220), 373–376.
Schmittner, A., Saenko, O., Weaver, A., 2003. Coupling of the hemispheres in observations and simulations of glacial climate change. Quat. Sci. Rev. 22 (5-7), 659–671.
Schönwiese, C.D., Walter, A., Brinckmann, S., 2010. Statistical assessments of anthropogenic and natural global climate forcing. an update. Meteorol. Zeitschrift 19 (1), 3–10.
Sedlacek, K., Knutti, R., 2012. Evidence for external forcing on 20th-century climate from combined ocean atmosphere warming patterns. Geophys. Res. Lett. 39 (20), L20708.
Shakun, J., Clark, P., He, F., Marcott, S., Mix, A., Liu, Z., Otto-Bliesner, B., Schmittner, A., Bard, E., 2012. Global warming preceded by increasing carbon dioxide concentrations during the last deglaciation. Nature 484 (7392), 49–54.
Sigman, D., Hain, M., Haug, G., 2010. The polar ocean and glacial cycles in atmospheric CO_2 concentration. Nature 466 (7302), 47–55.
Skinner, L., Fallon, S., Waelbroeck, C., Michel, E., Barker, S., 2010. Ventilation of the deep Southern Ocean and deglacial CO_2 rise. Science 328 (5982), 1147–1151.
Smirnov, D., Mokhov, I., 2009. From Granger causality to long-term causality: application to climatic data. Phys. Rev. E 80 (1), 016208.
Soon, W., Posmentier, E., Baliunas, S., 1996. Inference of solar irradiance variability from terrestrial temperature changes, 1880–1993: an astrophysical application of the sun-climate connection. Astrophys. J. 472 (2), 891–902.
Stocker, T., Johnsen, S., 2003. A minimum thermodynamic model for the bipolar seesaw. Paleoceanography 18 (4), 1087.
Stone, D., Allen, M., Selten, F., Kliphuis, M., Stott, P., 2007. The detection and attribution of climate change using an ensemble of opportunity. J. Climate 20 (3), 504–516.
Stone, D., Allen, M., Stott, P., Pall, P., Min, S.K., Nozawa, T., Yukimoto, S., 2009. The detection and attribution of human influence on climate. Annu. Rev. Energy Resour. 34, 1–16.
Stott, P., Tett, S., Jones, G., Allen, M., Ingram, W., Mitchell, J., 2001. Attribution of twentieth century temperature change to natural and anthropogenic causes. Clim. Dyn. 17 (1), 1–21.
Taylor, K., Stouffer, R., Meehl, G., 2012. An overview of CMIP5 and the experiment design. Bull. Amer. Met. Soc. 93 (4), 485–498.
Willeit, M., Ganopolski, A., Dalmonech, D., Foley, A., Feulner, G., 2014. Time-scale and state dependence of the carbon-cycle feedback to climate. Clim. Dyn. 42 (7-8), 1699–1713.
Zeebe, R., 2012. History of seawater carbonate chemistry, atmospheric CO_2, and ocean acidification. Annu. Rev. Earth Planet. Sci. 40, 141–165.
Zhang, Y., Yu, G., Yang, J., Wimberly, M., Zhang, X., Tao, J., Jiang, Y., Zhu, J., 2014. Climate-driven global changes in carbon use efficiency. Glob. Ecol. Biogeogr. 23 (2), 144–155.
Zickfeld, K., Eby, M., Weaver, A., Alexander, K., Crespin, E., Edwards, N., Eliseev, A., Feulner, G., Fichefet, T., Forest, C., Friedlingstein, P., Goosse, H., Holden, P., Joos, F., Kawamiya, M., Kicklighter, D., Kienert, H., Matsumoto, K., Mokhov, I., Monier, E., Olsen, S., Pedersen, J., Perrette, M., Philippon-Berthier, G., Ridgwell, A., Schlosser, A., Schneider von Deimling, T., Shaffer, G., Sokolov, A., Spahni, R., Steinacher, M., Tachiiri, K., Tokos, K., Yoshimori, M., Zeng, N., Zhao, F., 2013. Long-term climate change commitment and reversibility: an EMIC intercomparison. J. Climate 26 (16), 5782–5809.